JTTEE5 11:333-349

Mechanisms of Fatigue Failure in Thermal Spray Coatings

R. Ahmed and M. Hadfield

(Submitted 13 May 2001; in revised form 14 November 2001)

The aim of this experimental study was to ascertain the fatigue failure modes of thermal spray coatings in rolling/sliding contact. These failure modes outline the design requirements of thermal spray coatings for high-stress tribological applications including impact and point or line contact loading. Recently, a number of scientific studies have addressed the fatigue performance and durability of thermal spray coatings in rolling/sliding contact, but investigations on the mechanisms of these failures are seldom reported. The understanding of such failure mechanisms is, however, critical in optimizing the generic design of these overlay coatings. This study takes a holistic approach to summarize the results of ongoing research on various cermet (WC-Co) and ceramic (Al_2O_3) coatings deposited by detonation gun (D-Gun), high-velocity oxyfuel (HVOF), and high-velocity plasma spraying (HVPS) techniques, in a range of coating thickness (20-250 μm) on various steel substrates to deliver an overview of the various competing failure modes. Results indicate four distinct modes of fatigue failure in thermal spray cermet and ceramic coatings: abrasion, delamination, bulk failure, and spalling. The influences of coating process, thickness, materials, properties of substrate materials, and prespray conditions on these fatigue failure modes are also discussed. A modified four-ball machine was used to investigate these failure modes under various tribological conditions of contact stress and lubrication regimes in conventional steel and hybrid ceramic contact configurations. Results are discussed in terms of pre- and post-test surface examination of rolling elements using scanning electron microscopy (SEM), electron probe microscopy analysis (EPMA), and surface interferometry, as well as subsurface observations using x-ray diffraction (XRD), residual stress analysis, and dye-penetrant investigations.

Keywords cermet and ceramic overlay coatings, failure modes, rolling contact fatigue

1. Introduction

1.1 Industrial Context

Whenever an advanced material or manufacturing process is introduced into the design of components, the demand for higher efficiency and durability pushes the boundaries of the process to its limits. The economics of such an industrial process place further demands to consolidate the market share, and the process of thermal spraying is no exception to this tendency. Although technological advancements in surface engineering, such as hybrid ceramics[1] and vapor deposition techniques,[2] have increased the fatigue performance of such coatings for tribological applications in rolling/sliding contacts, the process economics have limited their use to specific applications. It is thus appreciated that thermal spray coatings can provide a cost-effective solution for these and other novel tribological applications. It is therefore not surprising that industrial demands have recently triggered a number of investigations relating to the durability of these coatings in rolling/sliding contacts.[3-5]

R. Ahmed, Heriot-Watt University, Department of Mechanical and Chemical Engineering, Riccarton, Edinburgh, EH14 4AS, United Kingdom; and **M. Hadfield,** Bournemouth University, School of Design, Engineering & Computing, Tribology Design Research Unit, Studland House, 12 Christchurch Road, Bournemouth, BH1 3NA, United Kingdom. Contact e-mail: r.ahmed@hw.ac.uk.

The technology of thermal spraying has come a long way in developing its niche and market share in surface engineering, especially in the area of tribological applications. The advantages of environmentally friendly processes, the choice of coating and substrate materials, and restoration of worn/undersized components have thus provided a thrust in expanding the boundaries of this technology. These investigations have indicated that the coating design, such as the choice of coating and substrate material, coating thickness, and tribological conditions play an important role in dictating the performance of these coatings. However, a generic design approach for these overlay coatings in concentrated rolling/sliding contacts demands a thorough understanding of the mechanisms of fatigue failure. To date, such investigations are seldom seen in published literature and only relate to a specific coating process or material. This investigation holistically approaches and categorizes the various fatigue failure modes and underpinning mechanisms on the basis of ongoing experimental investigation, which includes a number of coating processes, materials, substrate steels, coating thicknesses, and tribological conditions of stress, configuration, and lubrication.

1.2 State of Art—Analytical and Experimental Approach

The explicit nature of the thermal spraying process, resulting in a lamellar coating microstructure containing varying degrees of porosity and defects, makes the analytical approaches to determine and combat failure mechanisms, complex and expensive. He et al.[6] modeled the role of interfacial cracking in constrained metal layers for a ductile homogenous and isotropic

material. They indicated the importance of crack size and coating thickness on failure mode using a finite element code. Although these models give some insight to the behavior of crack propagation, results cannot be applied to thermal spray coatings in rolling/sliding contacts. This is because the composite and lamellar structure of thermal spray coatings make them brittle in nature, and because crack shapes are complex to model. In addition, loading at the interface is shearing in concentrated rolling/sliding contacts, whereas tensile loading is considered in these models. Liu et al.[7] recently addressed one of these problems by analyzing the thermal mismatch of the coating and substrate materials. However, only vapor-deposited coatings under the influence of thermal loading can be analyzed. Rammet al.,[8] however, considered an experimental approach for interfacial debonding of these coatings. Clearly, an experimental approach is a more reliable method to ascertain the failure modes and mechanisms of thermal spray coatings, because it considers the complexities of coating microstructure.

Previous studies by Yoshida et al.[9] and Nieminen et al.[10] on the fatigue behavior of thermal spray coatings in rolling or rolling/sliding contacts indicated that the performance is dependent upon the tribological conditions. However, the understanding of failure modes dictates the performance of current and future applications. This paper addresses failure modes by selecting a number of cases (Table 1) from a battery of experimental tests, and reveals not only the modes of fatigue failures, but also outlines the physical mechanisms leading to these failures.

2. Experimental Test Procedure

2.1 Thermally Sprayed Rolling Elements

This investigation considers thermal spray coatings deposited by three commercially available processes, i.e., detonation gun (D-Gun, SDG2040 Praxair-TAFA, USA), high velocity oxyfuel (HVOF, JP5000 Praxair-TAFA, USA), and high velocity plasma spraying (HVPS, GG-WC-102 Sermatech International, USA). The microstructure, residual stresses, and physical properties of these coatings depend upon the wettability, speed, temperature, and viscosity of impacting lamella, and thermal conductivity, temperature, and surface roughness of the underlying coating or substrate. These processes thus provided a range of average particle speeds and temperatures for this study. To minimize the effect of coating process conditions on the fatigue failure modes, industrially optimized process parameters for each of the coating processes were used in this investigation. Although Wilms et al.[11] and Kudinov et al.[12] investigated the behavior of impacting lamella and reported numerous features that (depending on the splat behavior) may exist within the coating microstructure, to date, no reliable physical model exists to relate the process parameters and coating microstructure.

The coating materials selected were WC-Co and Al_2O_3. This selection was made on the basis of high hardness and proven resistance to sliding wear.[13] These coatings were deposited in a thickness range of 20-250 μm. Coating thickness was varied to investigate the influence of location of shear stresses above or

Table 1 Rolling Contact Fatigue Test Results

Test Number	T1	T2	T3	T4	T5	T6
Coating process	D-Gun (SDG2040)	D-Gun (SDG2040)	HVOF (JP5000)	HVOF (JP5000)	HVOF (JP5000)	HVOF (JP5000)
Coating material	Al_2O_3	WC-15%Co	WC-12%Co	WC-12%Co	WC-12%Co	WC-12%Co
Coating thickness (μm)	70	60	150	50	20	110
Coating hardness (HV_{300})	1000	1100	1225	1390	1390	1380
Substrate steel	M-50 steel cone	440-C steel ball	Mild steel cone	Mild steel cone	Mild steel cone	M-50 steel ball
Substrate hardness (HV_{100})	725	600	218	218	218	803
Test lubricant	Hitec-174	Hitec-174	Exxon-2389	Exxon-2389	Exxon-2389	Hitec-174
Contact stress, P_o (GPa)	3.4	5.2	2.7	2.7	1.7	3.4
Planetary balls	Steel	Ceramic	Steel	Steel	Steel	Steel
Stress cycles	90×10^3	99×10^3	116×10^3	126×10^3	68×10^6	36×10^3
Failure mode (abrasive)	√				√	
Failure mode (delamination)	√	√				√
Failure mode (bulk failure)			√	√		
Failure mode (spalling)						

Test Number	T7	T8	T9	T10	T11	T12
Coating process	HVOF (JP5000)	HVOF (JP5000)	HVOF (JP5000)	HVOF (JP5000)	HVPS (GGWC)	HVPS (GGWC)
Coating material	WC-12%Co	WC-12%Co	WC-12%Co	WC-12%Co	WC-15%Co	WC-15%Co
Coating thickness (μm)	250	250	250	50	260	260
Coating hardness (HV_{300})	1296	1296	1296	1296	1190	1190
Substrate steel	440-C steel cone	440-C steel cone	440-C steel cone	440-C steel cone	440-C steel cone	440-C steel cone
Substrate hardness (HV_{100})	728	728	728	728	700	700
Test lubricant	Hitec-174	Hitec-174	Hitec-174	Hitec-174	Exxon-2389	Hitec-174
Contact stress, P_o (GPa)	3.7	2.7	3.1	3.1	2.7	2.7
Planetary balls	Steel	Steel	Ceramic	Ceramic	Steel	Steel
Stress cycles	13×10^3	70×10^6	30×10^6	0.7×10^6	4.3×10^6	38×10
Failure mode (abrasive)	√	√	√			√
Failure mode (delamination)				√	√	
Failure mode (bulk failure)						
Failure mode (spalling)	√					

below the interface during the contact loading. The substrate material was either 440-C, M-50 bearing steel, or mild steel in the shape of rolling element ball or cone. This enabled investigation of substrate hardness variations on the failure modes of thermally sprayed rolling elements. Bearing steel balls were commercial grade 12.7 mm diameter, whereas the rolling element cones were machined to 14.5 mm in diameter with apex angles of 90° and 109°. These variations in the substrate shape and cone angle affected the roll/slip ratio. Prior to the coating process, the substrate material was shot-blasted and preheated to increase the contact area for mechanical interlock and decrease the quenching stresses within the impacting lamella. Except for the M-50 steel substrate, for which the preheat temperature was lowered to 50 °C to avoid softening of substrate material, coatings were produced at a substrate preheat temperature of approximately 150 °C.

2.2 Rolling Contact Fatigue (RCF) Tests

A modified four-ball machine, as shown in Fig. 1, was used to investigate the RCF performance of thermally sprayed rolling elements. This modification allowed the rotation of the planetary-balls to correctly model the kinematics of rolling element bearings and precisely defined the contact load. Tourret and Wright[14] gathered various papers that describe various test results, ball dynamics, and kinematics. Investigations of lubrication effects by Scott and Blackwell[15] and recent studies on physical vapor deposition (PVD) coatings have also been performed by Sproul et al.[2] to evaluate the RCF performance using similar equipment. In the current setup, the coated rolling element cone or ball replaced the upper drive ball, which represented the inner race of the rolling element ball bearing. These coated rolling elements were ground and polished to attain a root mean square (RMS) surface roughness of 0.1 ± 0.05 μm (R_q). Details of the technique used to polish coated rolling elements can be seen in Ahmed and Hadfield.[16] Planetary balls were commercial grade 12.7 mm diameter 440-C bearing steel or hot isostatically pressed silicon nitride ceramic, with a surface roughness of 0.01 ± 0.005 μm (R_q). These two materials were used to conduct RCF tests in conventional steel ball bearing (steel planetary balls) and hybrid ceramic bearing (ceramic planetary balls) configurations. RCF tests were conducted under immersed lubrication conditions, at a spindle speed of 4,000 ± 10 rpm, and at an ambient temperature of 24 °C. Failure was defined as the increase in vibration amplitude above a preset level. Two test lubricants, i.e., Hitec-174 and Exxon-2389 were mainly used in the testing program. Hitec-174 is a high-viscosity hydrocarbon oil having a kinematic viscosity of 200 mm^2s^{-1} at 40 °C. Exxon-2389 is a commercially available synthetic oil having a kinematic viscosity of 12.4 mm^2s^{-1} at 40 °C. The ratio of the elasto-hydrodynamic lubricant (EHL) film thickness to average roughness (λ) was calculated using the following relation:

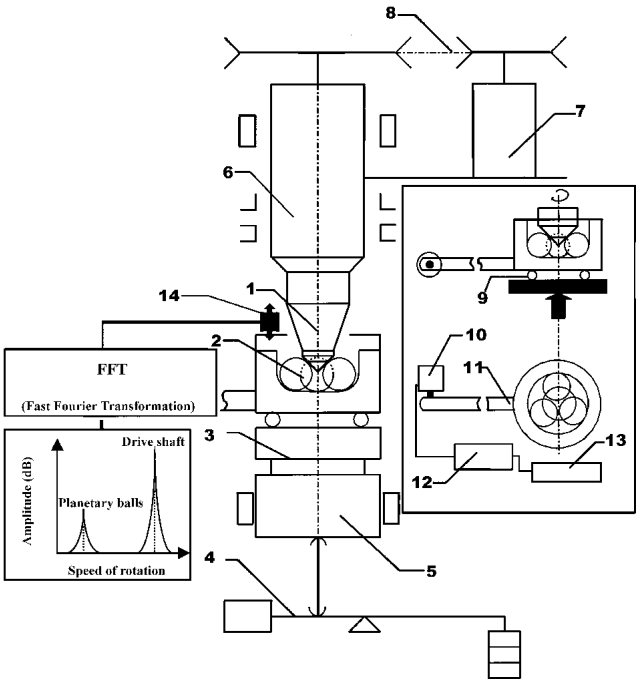

Fig. 1 Schematic of modified four ball machine: **(1)** coated cone and collet; **(2)** planetary balls; **(3)** heater; **(4)** loading lever; **(5)** loading piston; **(6)** spindle; **(7)** driving motor; **(8)** belt drive; **(9)** thrust bearing; **(10)** force transducer; **(11)** torque arm for friction measurements; **(12)** digital readout; **(13)** printer; **(14)** accelerometer

$$\lambda = H_{min}/(R^2_{qd} + R^2_{qp})^{0.5} \quad \text{(Eq 1)}$$

where R_{qd} is the RMS surface roughness of the driving rolling element, R_{qp} is the RMS surface roughness of the planetary ball. H_{min} is the minimum film thickness, calculated using the following relationship of hard EHL,[17] reproduced here for clarity:

$$H_{min} = 3.63\ U^{0.68}\ G^{0.49}\ W^{-0.073}\ (1 - e^{-0.68k}) \quad \text{(Eq 2)}$$

where U is the dimensionless speed parameter, G is the dimensionless material parameter, W is the dimensionless load parameter, and k is the dimensionless ellipticity parameter. The λ value was approximated as $\lambda > 3$ and $3 > \lambda > 1.5$ for the Hitec-174 and Exxon-2389 lubricants, respectively. In addition to these lubricants, RCF tests were also conducted dry and using a 50% mixture by volume of brake fluid and distilled water, and also using dye penetrant as a test lubricant. The modified four-ball machine was also instrumented to investigate the gross sliding in the four-ball system and to measure the total frictional torque in the cup assembly (details of these techniques can be seen in Ahmed and Hadfield[18,19]).

2.3 Residual Stress Measurements

Residual stress measurements of the rolling elements before and after the RCF tests were performed using x-ray diffraction (XRD). Ahmed and Hadfield[20] gave a detailed description of the generation of residual stress in thermal spray coatings. This technique can accurately measure the magnitude and orientation of both macro and micro residual stresses, but suffers from low penetration depth in materials such as WC. The $\sin^2$ technique of XRD was used, which makes use of the Bragg's equation:

$$n\xi = 2d \sin \quad \text{(Eq 3)}$$

$$\varepsilon = \frac{\Delta d}{d} = \cot\theta_d \Delta\theta \quad \text{(Eq 4)}$$

where n is the positive integral number indicating the order of diffraction, ξ is the x-ray wave length, d is the interplanar spacing in the crystal, θ is the diffraction angle, ε is the quantity of strain, and θ_d is the diffraction angle in a stress-free condition. A detailed description of residual stress measurement by XRD can be found in Farrahi et al.[21] The elastic constant (K) value for these measurements was measured using conventional in situ four-point bending test equipment subjected to a known stress within the elastic range. The details of the method were described by Cullity[22] and the measured value was −466 MPa/°. Cr-Kα was used as the x-ray source and the depth of penetration was approximated as 3 μm. The measurement plane (h, k, l) was (1, 0, 2).

3. Experimental Results

3.1 RCF Test Results

RCF tests were conducted in a variety of tribological conditions of contact stress, lubrication, and contact configuration on various coating thicknesses and substrate materials. Table 1 summarizes typical tribological test conditions and RCF results. Results summarized in Table 1 are selected from a battery of tests to comprehend the performance and ascertain the failure modes under various tribological conditions, and are not intended for statistical fatigue life prediction. Values of peak compressive Hertzian stress (P_o) listed in Table 1 are based on the uncoated case of rolling elements for various reasons discussed later in Section 4.2. These stresses were values calculated using the following relation:

$$P_o = \frac{3F}{2\pi ab} \quad \text{(Eq 5)}$$

where a and b are the major and minor axis of Hertzian contact ellipse, respectively, which can be calculated from Young's modulus and Poisson's ratio of the rolling elements,[23] and F is the contact force, calculated using the relation

$$F = \frac{9.8RM}{3\cos(\theta)} \quad \text{(Eq 6)}$$

where R is the lever arm ratio of the modified four ball machine set at 20:1, M is the mass at the end of lever arm, and θ is the angle of contact between the drive and driven rolling element.

3.2 Surface Observations of Failed Rolling Elements

Figure 2 shows the surface of a failed Al_2O_3-coated cone (test T1, Table 1) subjected to a stress of 3.4 GPa. Figure 2(a) shows the overall view of the failed area. This rolling element failed at the coating substrate interface, which was further confirmed by electron probe microscopy analysis (EPMA). This figure shows that the coating failure was parallel to the surface of the rolling element. The depth of failure was approximated as 70 μm. Figure 2(b) shows the damage within the wear track at a different location.

Figure 3 shows the surface observation of a D-Gun-coated WC-15%Co-coated rolling element ball (test T2). The coated rolling element was tested at a much higher (than T1) contact stress of 5.2 GPa and failed from within the coating microstructure. This was confirmed by EPMA analysis and by sectioning of the rolling element. Figure 3(a) shows a view of the failed area. In addition to this failure, the wear track of this coated

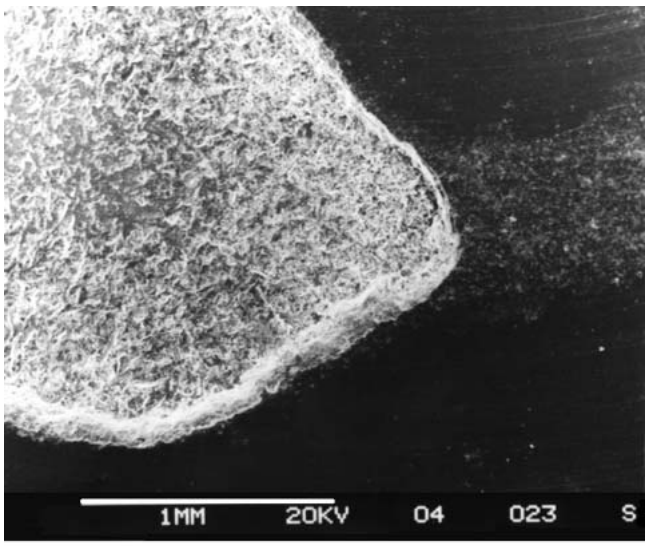

(a)

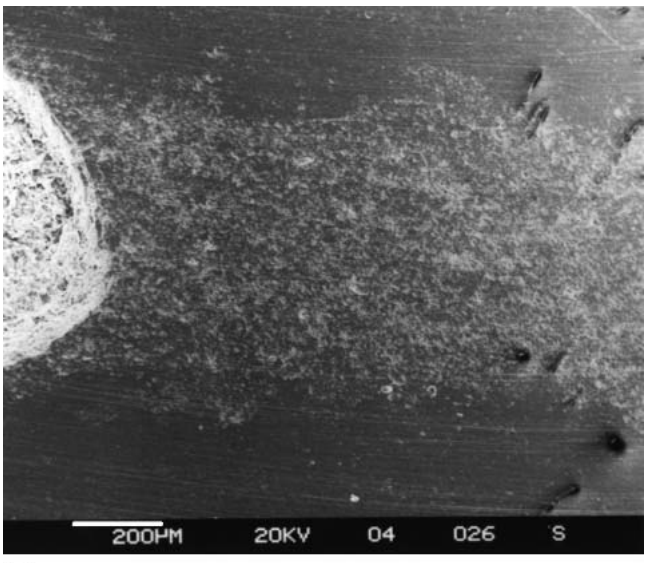

(b)

Fig. 2 Surface observations of Al_2O_3 coating produced by D-Gun technique on M-50 steel substrate (test T1): **(a)** leading edge of failed area; **(b)** wear track

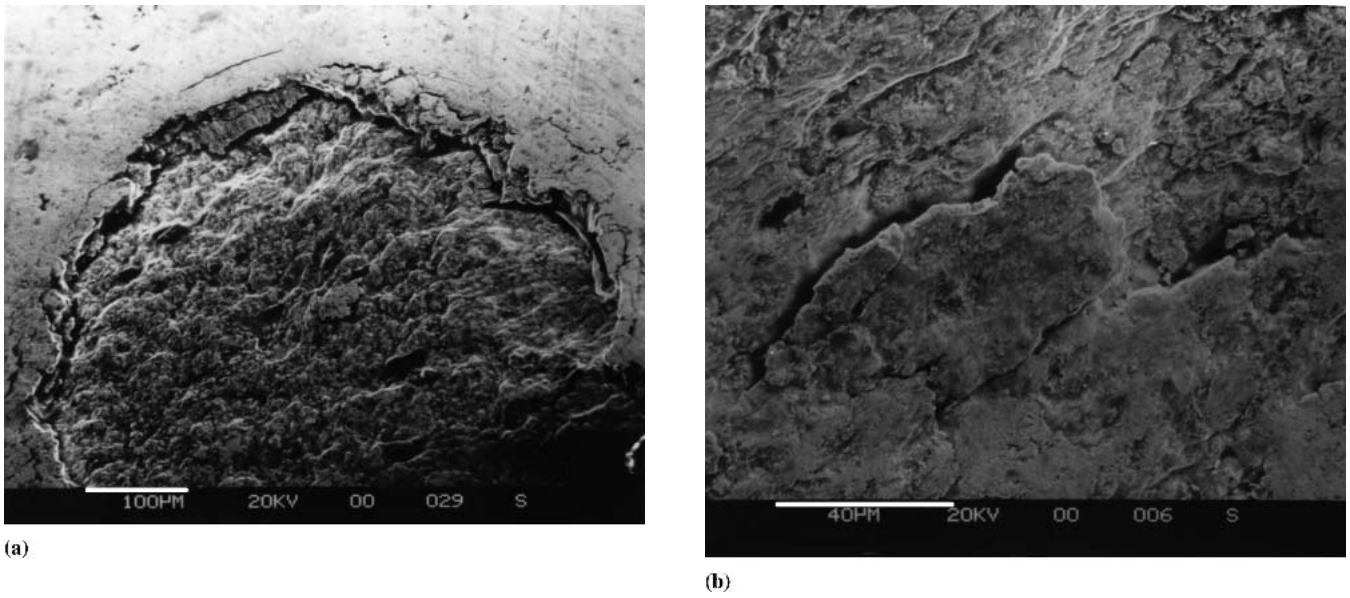

Fig. 3 Surface observation of WC-15%Co coating produced by D-Gun technique on 440-C steel substrate (test T2): **(a)** overall view of the failed area; **(b)** cracks and loose debris in the wear track

rolling element had numerous pits, as shown in Fig. 3(b). This figure also shows some loose debris about to detach from the coating surface.

Figure 4 shows the surface observations of failed HVOF coated rolling elements on mild steel substrate (test T3, T4, and T5). Figure 4(a) shows the cracks observed on the surface of coated cone after 126×10^3 stress cycles. This rolling element had a coating thickness of 150 μm and was tested at a contact stress of 2.7 GPa (test T3). The cracks appeared at the edge and in the middle of the wear track, which led to the failure of the coated rolling element. Figure 4(b) shows the surface observation of a similar rolling element tested under similar tribological conditions (as T3), but had a reduced coating thickness of 50 μm. This rolling element showed a migration of substrate to the surface through the cracks in the middle and at the edge of the wear track, as shown in Fig. 4(b) in the back-scattered image (BEI) (test T4). Figure 4(c) shows these transgranular cracks in the middle of the wear track at a high magnification. A similar trend was observed for relatively thinner 20 μm coatings, tested at contact stress of 2.7 GPa. The coating cross section also confirmed the plastic deformation and cracking of substrate material. However, when 20 μm thick coatings were tested at a lower contact stress of 1.7 GPa with Hitec-174 as the test lubricant (test T5), not only did the number of stress cycles to failure increase to 68.5×10^6, but also the failed rolling element showed no signs of cracking or plastic deformation. The wear track, however, showed the appearance of micropits, as shown in Fig. 4(d).

Figure 5 shows typical surface observations of a failed rolling element, coated at a low preheat temperature of 50 °C to avoid the softening of substrate M-50 steel (test T6). Figure 5(a) shows the overall view of the failed coated rolling element tested at a contact stress of 3.4 GPa using Hitec-174 as the test lubricant in conventional steel ball bearing configuration. The failure was in the first few thousand stress cycles, at the coating substrate interface. Figure 5(b) shows at a higher magnification the cracks radiating from the wear track. A test at a lower contact stress (2.1 GPa) did not show fatigue failure up to 52.4×10^6 stress cycles, but some micropits appeared, similar to those shown in Fig. 4(d).

Figure 6 shows the surface observation of 250 μm thick HVOF coating on 440-C bearing steel substrate cone (test T7-T10). Figure 6(a) shows the overall view of the wear track. This sample was tested at a contact stress of 3.7 GPa in Hitec-174 lubricant (test T7). The failure was within the coating microstructure, which was confirmed by EPMA analysis. Figure 6(b) shows the wear track of a similar specimen tested at a reduced contact stress of 2.7 GPa (test T8). The failed area of the wear track in a similar test, but in hybrid ceramic bearing configuration, is shown in Fig. 6(c) (test T9). Figure 6(d) shows the failure of a 50 μm thick coated rolling element tested under similar conditions of contact stress and test configuration (test T10).

Figure 7 shows the surface observation of test specimen produced by the HVPS technique (test T11 and T12). Figure 7(a) shows the overall view of the failed area. This specimen was tested at a contact stress of 2.7 GPa in Exxon-2389 lubricant (test T11). The depth of failure was approximated as 50 μm. Figure 7(b) shows the wear track of a similar test conducted with Hitec-174 lubricant (test T12).

3.3 Subsurface Observations of Failed Rolling Elements

Subsurface observations were carried out using fluorescent dye microscopy to ensure that any cracks observed were caused by the RCF tests and not the sectioning process. Details of the technique are described in Ahmed and Hadfield.[5] Figure 8 shows typical subsurface cracks parallel to the wear track for the HVPS and HVOF WC-Co coatings. Figure 8(a) shows the subsurface cracks at the edge of the wear track for the test specimen shown in Fig. 7 (test T11). Two subsurface cracks were visible at the approximate depths of 40 and 90 μm. Further sectioning into

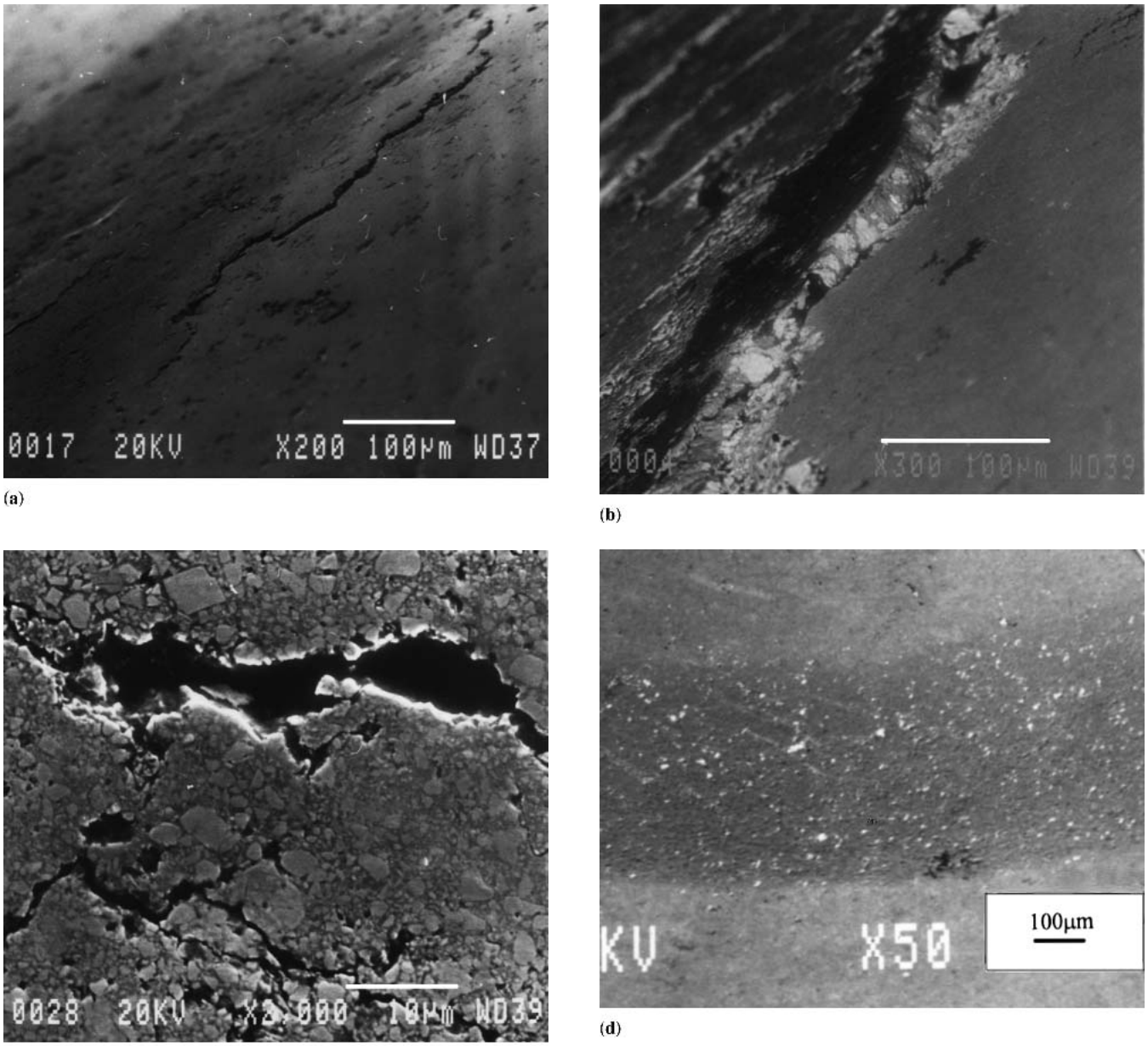

Fig. 4 Surface observation of WC-12%Co coating produced by HVOF technique on mild steel substrate (test T3, T4, T5): **(a)** cracks at the edge of wear track (test T3); **(b)** substrate emerging at the edge of wear track (test T4); **(c)** intergranular cracks in the middle of wear track (test T4); **(d)** wear track (test T5)

the wear track showed that these cracks joined each other and a new crack appeared at approximate depth of 90 µm within the wear track (Fig. 8b). Toward the middle of the wear track, the crack became circumferential and extended to about 7 mm in length, as shown in Fig. 8(c). However, the failure was actually due to a crack at another location at a dept of 50 µm, as shown in Fig. 8(d). A similar trend was seen in HVOF coatings, as shown in Fig. 8(e). This HVOF-coated sample had a coating thickness of 250 µm and was tested under conditions similar to those for test T11. Subsurface cracks appeared at the edge of the wear track, which extended to greater lengths within the wear track, as shown in Fig. 8(f). The cracking behavior was different for coating thickness less than 100 µm. In these cases, the cracks were generally seen at the coating substrate interface, as shown in Fig. 8(g) for the HVPS coating. This specific sample had a coating thickness of 80 µm and was tested at a contact stress of 2.7 GPa. Figure 8(h) shows similar interfacial cracks at another location.

4. Discussion

Classification of fatigue failures was made on the basis of surface and subsurface observations of the failed rolling elements. Because the modified four ball machine is run at high

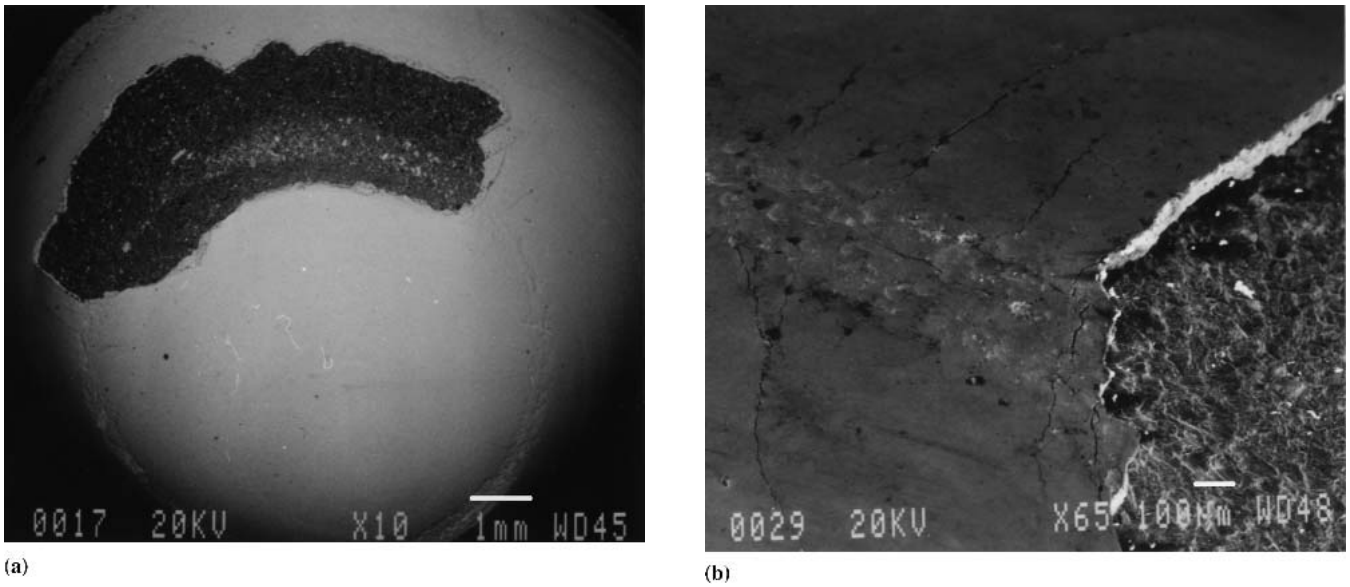

(a) (b)

Fig. 5 Surface observation of WC-12%Co coating produced by HVOF technique on M-50 steel substrate (test T6): **(a)** overall view of the failed area; **(b)** cracks radiating from wear track

speed, it is difficult to observe crack propagation. Post-test examination is the only method to ascertain failure modes and mechanisms. This classification of failure modes in thermal spray coatings in concentrated rolling contact is summarized in Table 2. These failures have been categorized into four main modes: abrasion, delamination, bulk failure, and spalling (M1-M4), as discussed below.

4.1 Abrasive Failure of Coated Rolling Elements

Micropitting and surface wear were observed under all tribological conditions considered in the experimental program. This failure mode was seen with both ceramic (Al_2O_3) and cermet (WC-Co) coatings and with all coating techniques considered. In some cases this was the only failure mode, as shown in Fig. 4(d), 6(b,c), and 7(b), whereas in other cases, micropitting and surface wear on the wear track were appreciable in combination with other modes of failure, as shown in Fig. 2, 5(b), and 6(a). Noncontacting three-dimensional interferometry of the wear track confirmed that these pits were up to 50 µm wide and a maximum of 5 µm deep. Littmann et al.[24] characterized similar failure as "peeling" during a study of fatigue failure modes of conventional steel ball bearings, whereas Tallian[25] characterized this type of failure as surface distress. Littmann[26] also used terms such as frosting and glazing, because of the dull appearance of affected areas, as shown in Fig. 7(b). Despite the various terminologies used, this behavior is generally associated with asperity contact in the presence of microslip within the contact region. Gross sliding, though not necessary for this type of failure, is thought to promote micropitting.

4.1.1 Mechanism of Coating Abrasion in Rolling/Sliding Contacts. For thermal spray coatings, a similar mechanism of asperity contact in the presence of microslip and sliding was responsible for the micropitting and surface wear. During partial EHL conditions, i.e., when the lubrication regime was in the mixed region ($1 < \lambda < 3$), surface asperities came into contact. Johnson et al.[27] has shown that under these conditions, the asperity contact and the EHL film share the load. According to Berthe et al.,[28] these asperity contacts produce high-stress concentrations very close to the surface, but do not change the subsurface Hertzian stress pattern. These stress concentrations, which are due to the interaction of asperities in the presence of microslip within the contact region, result in a shear stress beneath the asperity. Hard coatings such as WC-Co and Al_2O_3 respond to this stress concentration by microcracking. An example of such behavior is shown in Fig. 9(a), which shows the occurrence of these microcracks within the wear track of a WC-Co coating produced by the HVPS technique, tested at a contact stress of 3.1 GPa with ceramic planetary balls and Exxon-2389 lubricant, after 0.6 million stress cycles. A similar trend in microcracking at an advanced stage is shown in Fig. 3(b), in which loose debris is about to detach from the surface. Figure 9(b) shows the cross section of similar debris at an incipient detachment state; the depth of the resulting pit can be approximated as 2 µm, which is typical of the depth of pits obtained from noncontacting interferometry of the wear track. The microcracks can be seen as intergranular through the cobalt matrix. This microcracking also resulted in the attenuation of near-surface compressive residual stress within the coating material, as discussed in Section 4.5. Although plastic deformation of the coating material is possible, difficulties in sample preparation of hard WC-Co or Al_2O_3 coatings for TEM analysis have so far hindered the investigation to confirm plastic deformation.

Apart from the mechanism of asperity deformation leading to micropitting of the surface, the criterion of maximum tensile stress at the edge of the contact area for brittle materials also needs to be considered for thermal spray cermet and ceramic coatings. These stresses are very sharply localized and decay very rapidly at small depths below the surface. For elliptical con-

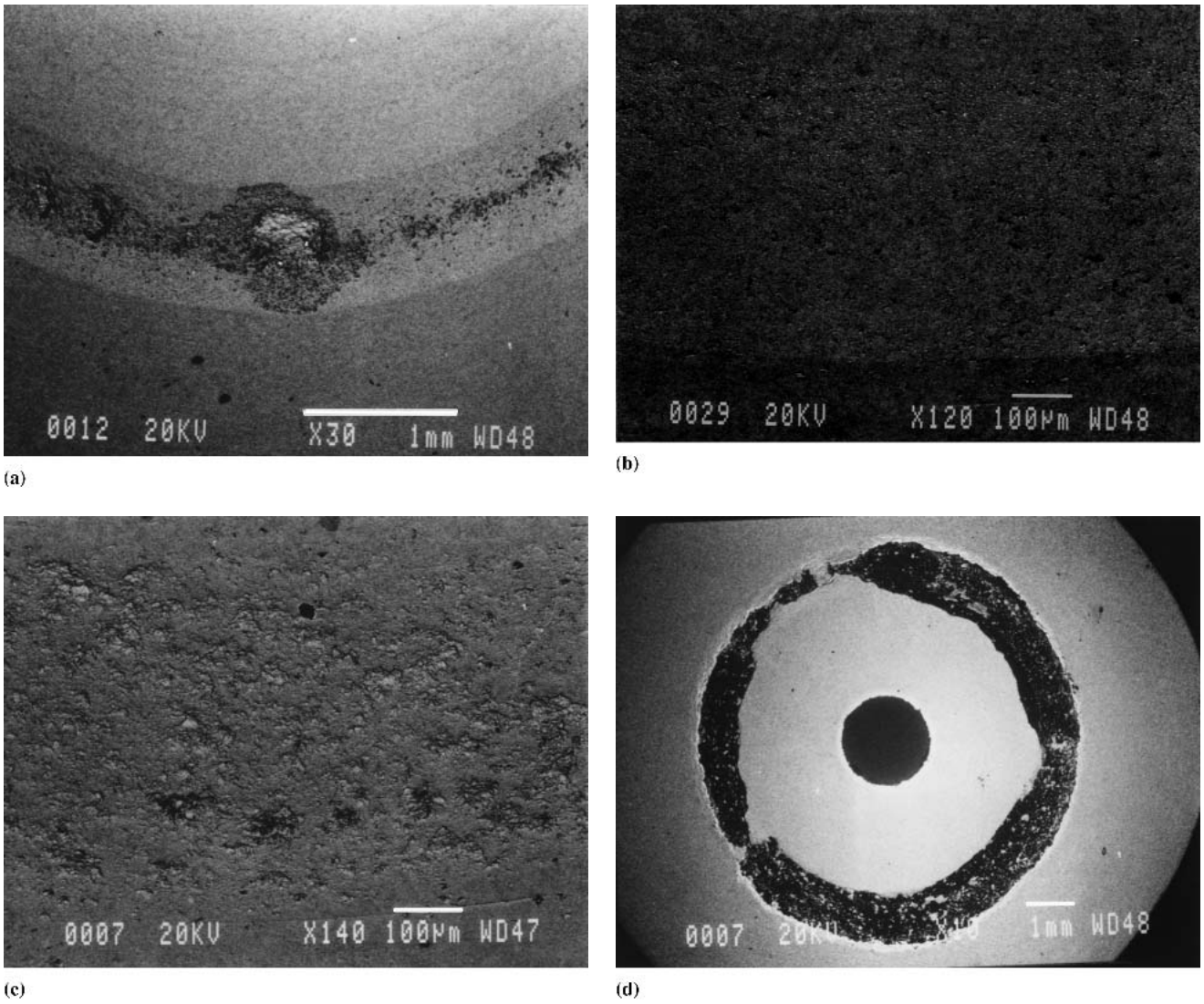

Fig. 6 Surface observation of WC-12%Co coating produced by HVOF technique on 440-C steel substrate (test T7, T8, T9, T10): **(a)** failed area (test T7); **(b)** overall view of wear track (test T8); **(c)** overall view of wear track (test T9); **(d)** failed area (test T10)

tacts, this tensile stress (T_{max}) for a given value of peak compressive stress P_o can be evaluated from the following relation reproduced here for clarity:[29]

$$\frac{T_{max}}{P_o} = \frac{0.33\beta}{n^3}\left[0.5 \ln\left(\frac{1+n}{1-n}\right) - n\right] \quad \text{(Eq 7)}$$

where β is the ratio of minor to major axis of contact ellipse, and $n = (1 - \beta^2)^{0.5}$. For the test conditions used in the test program, T_{max} was approximated as 324 MPa at a maximum compressive contact stress of 2.7 GPa. Tucker[30] showed that the fracture stress of WC-Co coatings using the technique of tensile test (free-standing ring) is in the range of 380-690 MPa for HVPS and D-Gun coatings. These values of fracture stress are similar to the tensile stresses associated with the Hertzian stress distribution at the edge of the contact region. This indicates that even under the fully developed EHL ($\lambda > 3$) regime, the microcracks in the coating material, caused either by coating defects or asperity contact, can propagate because of tensile stressing at the edge of the contact area. Coating fracture toughness also needs to be considered along with tribological test conditions while combating a coating's abrasive failure. Although no reliable method of evaluating the fracture toughness of thermal spray coatings exists to date,[31] the authors made a comparative analysis using the Vickers microhardness indentations technique.

Coatings produced by D-Gun and the Plasma Spray (APS) technique failed readily at an indentation load of 0.98-2.94 N, whereas HVOF coatings generally required a load of 4.9 N or more to fracture the surface (Fig. 12). On the basis of tensile stress criterion, it can be argued that one should expect relatively intense microcracking and eventually micropitting of D-Gun and HVPS coatings in comparison to HVOF coatings under similar test conditions. The difference in micropitting can be appreciated by comparing Fig. 6(b) and 7(b). Although the tribological conditions were similar for the two tests, micropitting was extensive for HVPS coating even after half the stress cycles in comparison to HVOF coatings (Table 1).

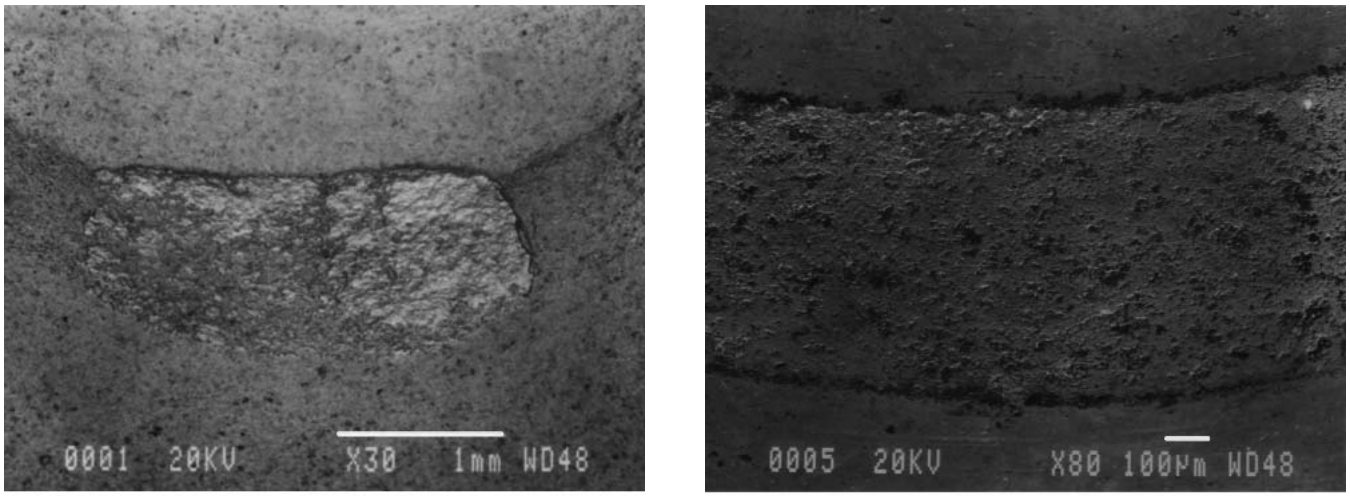

(a) (b)

Fig. 7 Surface observation of WC-15%Co coating produced by HVPS technique on 440-C steel substrate (test T11, T12): **(a)** failed area (test T11); **(b)** wear track (test T12)

The process of microfracture and surface wear was found to accelerate at the later stages of RCF testing because of the introduction of initial wear debris into the contact region, leading to three-body abrasion. Small-sized wear debris were produced during this process, as shown in Fig. 9(c). The composition of these wear debris was similar to that of the coating material for the tests conducted with ceramic lower balls, but with a small proportion of bearing steel material for tests with steel lower balls. The presence of these initial wear debris within the test lubricant was further confirmed by manually stopping the test prior to fatigue failure, and checking the lubricant for wear debris. Further tests using a splash-feed lubrication system by Ahmed and Hadfield[18] to remove the wear debris indicated an increase in the lifetime to failure by reducing the effect of three-body abrasion. Dents were also seen in the wear track at advanced stages of tests, which confirmed the presence of debris in the contact region. Note that three-body abrasion influenced the rate of micropitting for tests in both conventional and hybrid ceramic configurations because the wear debris were predominantly that of coating material, and hence, were of similar or higher hardness (because of the flash temperature) compared to that of the contacting pair. The specific analysis of the influence of size, shape, and composition of coating debris within the rolling contact region on micropitting of thermal spray coatings was, however, beyond the scope of this work. Readers are referred to work by Sayles[32] for a discussion of these factors.

4.1.2 Influence of Contact Pair Hardness. The extent of micropitting was also sensitive to the difference in hardness of interacting asperities. When RCF tests were conducted in a hybrid ceramic bearing configuration, the higher hardness of ceramic balls (HV_{300} = 1580) resulted in severe microcracking of the coating material (HV_{300} = 1100). The ceramic planetary balls underwent negligible wear during this process; no appreciable damage was seen on the surface of ceramic balls. The absence of silicon in the wear debris collected after the tests further confirmed that the coating material was predominantly removed with negligible ceramic material removal. One should expect a reverse trend for the tests performed with steel lower balls (HV_{100} = 820) because of their lower hardness compared the coating material, i.e., coating asperities should deform and flatten the asperities on steel planetary balls. Figure 6(b) and (c) highlights this point, and shows a comparison of the extent of micropitting for similar tests on HVOF, deposited WC-Co coating with steel and ceramic planetary balls. Figure 6(b) shows negligible amount of micropitting for a test suspended after 70×10^6 stress cycles, whereas Fig. 6(c) shows severe micropitting after 30×10^6 stress cycles with ceramic lower balls. This is consistent with the studies by Oliver et al.,[33] which demonstrated that the difference in hardness of interacting bodies is important in controlling the rate of wear produced by micropitting. However, one might have expected no evidence of micropitting with steel planetary balls, but a negligible amount was confirmed, which could be attributed to three-body abrasion. Plastic deformation was also seen on the surface of lower steel balls. This indicated that although higher hardness of coating asperities plastically deformed the lower steel balls, the shear stress at the root of the coating asperities was above the fracture toughness of the coating material, leading to cracking and eventually micropitting within the coating wear track.

4.1.3 Influence of Lubrication Regime. Although the consequence of asperity contact leading to microcracking is understood as microcracking, the influence of crack propagation resulting from hydraulic pressure propagation (HPP) proposed by Way[34] needs to be considered. It is proposed that HPP did not influence the micropitting of coatings. RCF tests conducted in the absence of lubricant confirmed this behavior. A comparison of the wear track of the failed rolling element for dry tests with lubricated tests showed that, although micropitting was severe for dry tests, the appearance of pits was similar in both cases, as shown in Fig. 9(d). This showed that the mechanism of surface pitting, i.e., asperity contact, was similar in both cases, with the only difference being the rate of abrasion.

The fracture toughness of the coating and the hardness of contacting asperities were thus the key factors controlling the micropitting in partial EHL conditions. It is debatable that this

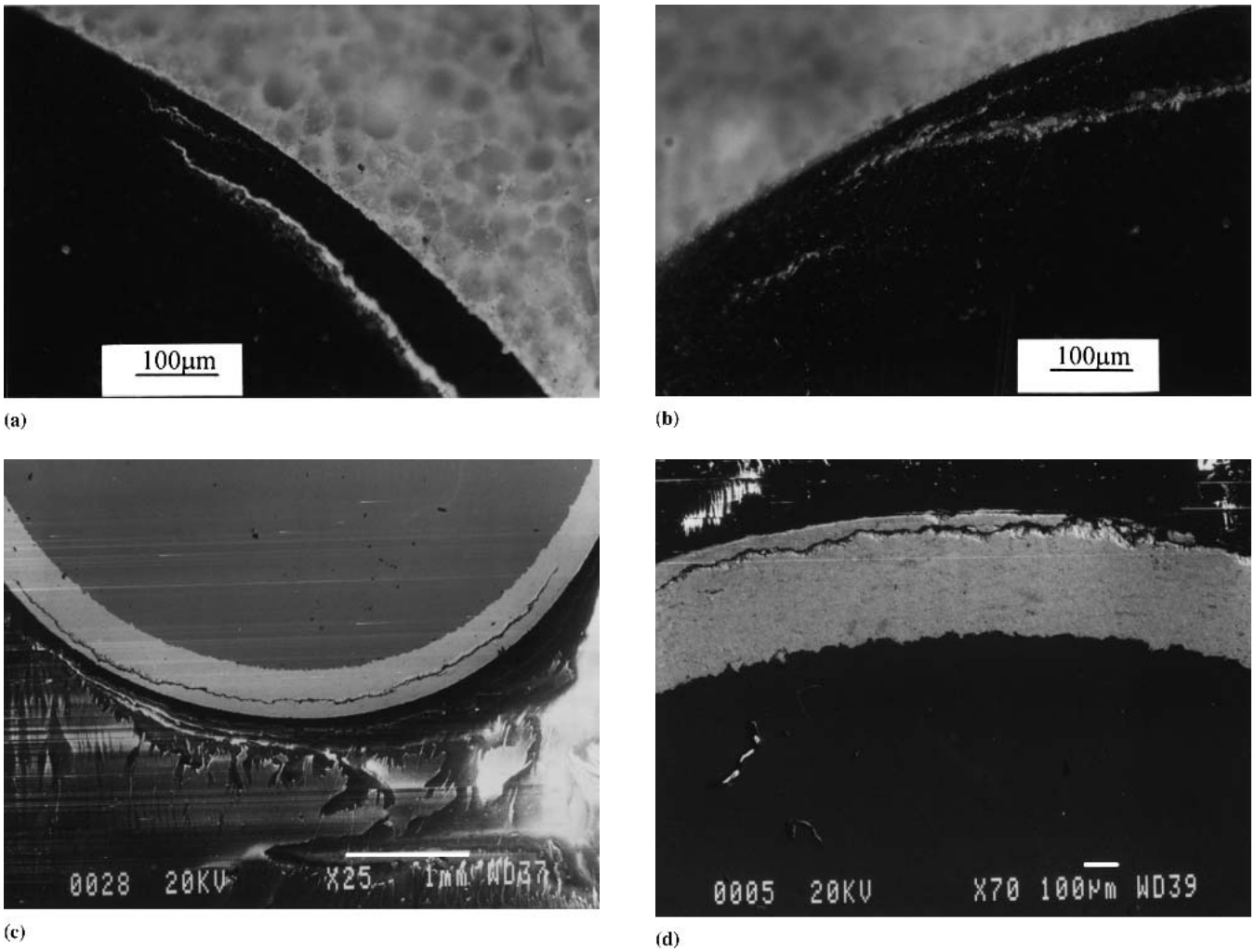

Fig. 8 Subsurface observation of WC-Co coating produced by HVPS and HVOF technique on 440-C steel substrate: **(a)** cracks at the edge of wear track (test T12, HVPS coating); **(b)** joining of cracks, (test T12, HVPS coating); **(c)** circumferential cracks, (test T12, HVPS coating); **(d)** failed area, (test T12, HVPS coating) (continued on next page)

type of failure should have been eliminated with Hitec-174 lubricant ($\lambda > 3$), i.e., for full film lubrication. The surface observations, however, confirmed that the failure mode was operational with all of the test lubricants. This is because although the λ ratio is a useful index to evaluate the tendency of surface wear and microcracking caused by the asperity contact, it could be misleading because of the brittle nature of thermal spray coatings; few asperity peaks above the RMS height can result in microcracking and can generate initial wear debris. Other parameters such as peak-to-valley depth or maximum peak height also need to be considered for such analysis. One way to confirm the extent of asperity contact is to compare the coefficient of rolling friction in partial and fully developed EHL. Still, it is impractical to evaluate the friction coefficient in the modified four-ball machine, frictional torque data from the cup assembly were used by the authors for comparative analysis.[19,35] This comparison of frictional torque in the four-ball assembly for lubricated tests did not show appreciable variations for lubricants (typical values of 0.02-0.05 Nm). This indicated that frictional conditions were similar despite the variations in λ value. The dry test, however, showed twice the frictional torque in the early stages of the test and then an order of magnitude higher at later stages (0.17 Nm) because of debris accumulation within the cup assembly. This indicated that variations in λ influence the performance and the rate of abrasive wear of coated rolling elements, but not the mechanism of micropitting.

In summary, regardless of the changes in coating material and spray processes considered within this study, tribological conditions and coating fracture toughness dictated the mechanism and rate of abrasive wear. A combination of factors, i.e., asperity contact and tensile stress at the edge of contact region, coupled with microslip sliding within the contact region, generated initial wear debris in two-body abrasion at a rate that was depended upon the lubrication regime and hardness ratio of the contacting pair. During the later part of the RCF test, the mechanism of three-body abrasion accelerated the process of abrasive wear, which is consistent with previous studies by Ahmed et al.[5] for plasma-sprayed coatings.

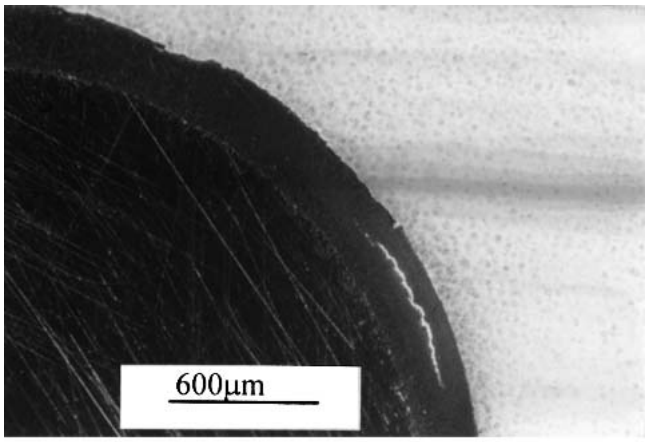

(c)

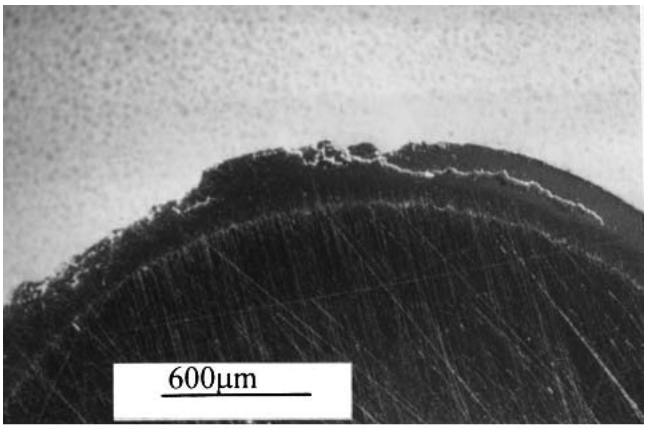

(f)

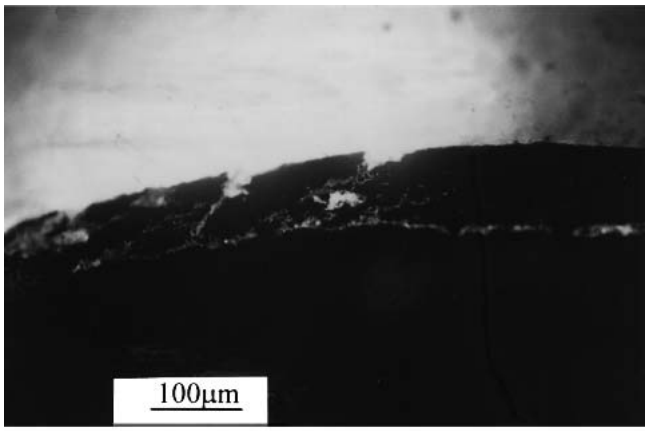

(g)

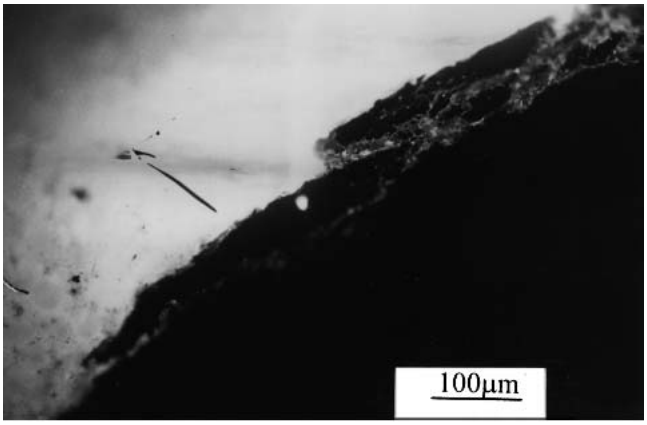

(h)

Fig. 8 cont. Subsurface observation of WC-Co coating produced by HVPS and HVOF technique on 440-C steel substrate: **(e)** cracks at the edge of wear track, (HVOF coating); **(f)** failed area (HVOF coating); **(g)** interfacial cracks (HVPS coating); **(h)** joining of cracks leading to failure (HVPS coating)

Table 2 Fatigue Failure Modes of Thermally Sprayed Cermet (WC-Co) and Ceramic (Al_2O_3) Coatings in Rolling/Sliding Contact

Failure Mode	Failure Mechanism	Failure Type
Abrasion (M1)	Asperity contact	Surface wear
	Microfracture and two-body abrasion	(M1a), (Fig. 4d, 6b)
	Wear acceleration due to three-body abrasion	Micropitting
	Small wear debris (a few microns in dimension)	(M1b) (Fig. 7b)
Delamination (M2)	Stress concentrations due to coating defects	Delamination at interface (M2a)
	Initiation of subsurface cracks	(Fig. 2, 6c)
	Crack propagation at the depths of shear stress	Delamination within microstructure
	Sheet-like thin debris (a few millimeters in dimension)	(M2b) (Fig. 3a, 7a)
Bulk failure (M3)	Yielding of substrate material	Cracks within wear track
	Migration of substrate to the edge of wear track	(M3a) (Fig. 4a,c)
	Intergranular cracking of coating within wear track	Migration of substrate
	No debris generated	(M3b) (Fig. 4b)
Spalling (M4)	Surface or subsurface crack initiation	Spalling
	Crack propagation due to cyclic loading	(M4) (Fig. 6a)

4.2 Delamination Failure of Coated Rolling Elements

Suh initially proposed a delamination theory of sliding wear in 1973. Suh,[36] Fleming and Suh,[37] Suh and Saka,[38] and Suh[39] have since performed experimental and theoretical analysis supporting the delamination theory. The mechanism of delamination wear includes the propagation of cracks parallel to the surface at a depth governed by material properties and the friction coefficient. Although rolling friction prevails in modified four ball tests and delamination theory is based on sliding friction, the similarities of the failure mechanisms in both cases

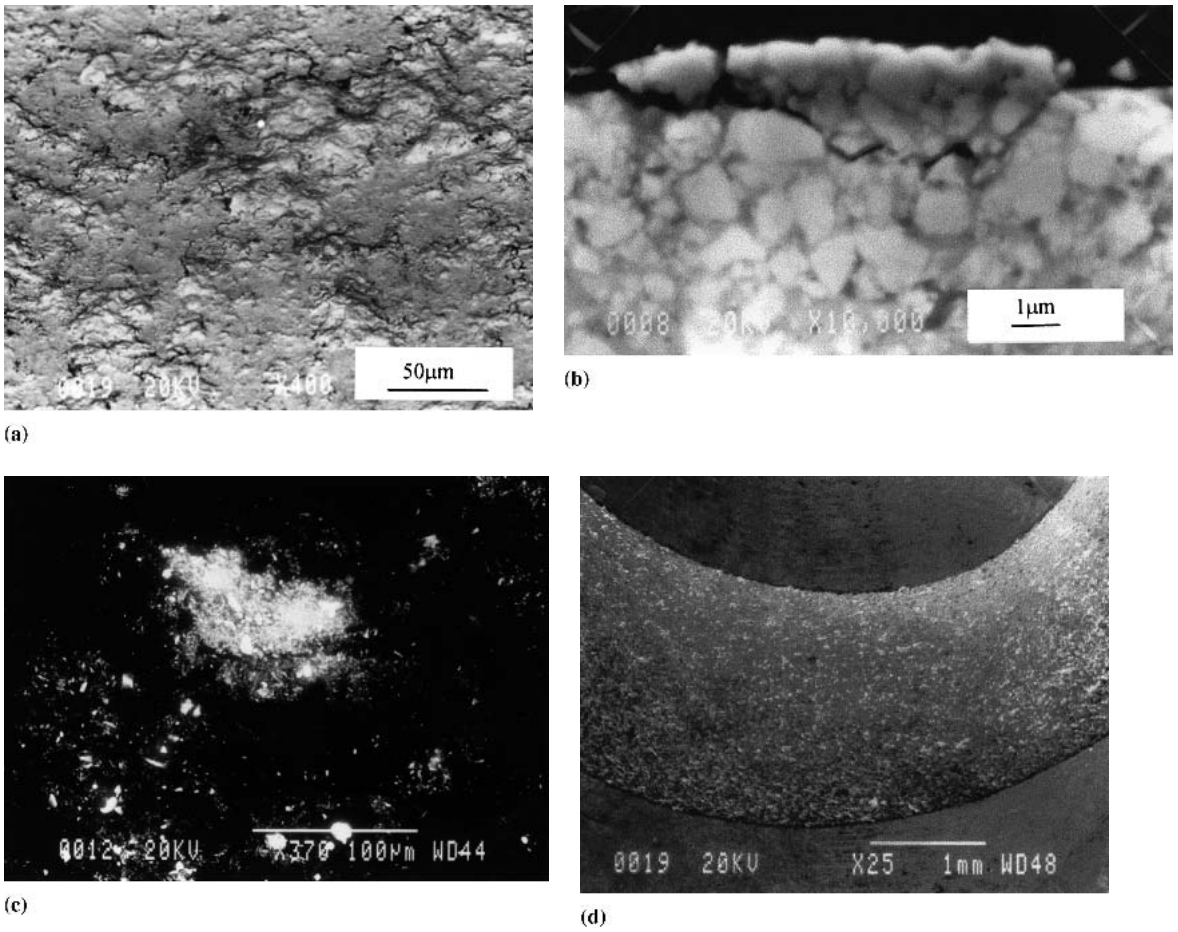

Fig. 9 Microcracks and debris leading to abrasive failure in WC-Co coatings: **(a)** microcracks within the wear track; **(b)** cross section of wear track; **(c)** debris from tests T12; **(d)** wear track of dry test

are compelling. Typical observation of coating delamination at the coating substrate interface can be seen from Fig. 2 and 6(d) for the Al_2O_3 and WC-Co coatings, respectively, whereas the delamination failure within the coating material can be seen in Fig. 3(a) and 7(a). Al_2O_3 coatings, however, did not show delamination within the coating material, but only at the coating substrate interface. Sheet-like debris, which reached a few millimeters in dimensions, were produced during this process as shown in Fig. 10(a) for WC-Co coating (test T6), whereas delamination debris for Al_2O_3 coatings were similar in shape and size to WC-Co coatings.

4.2.1 Mechanism of Coating Delamination in Cermet and Ceramic Coatings. The damage theory of materials begins with the premise that a material contains a multitude of defects in the form of microvoids,[40] which undergo extension because of loading and unloading. A similar approach is adapted to explain the mechanism of coating delamination. Coating microstructure contains varying levels of micropores, microcracks, and secondary phase particles, which act to concentrate stress during cyclic loading. A typical example of these defects for D-gun coating can be seen from Fig. 10(b). The extent of these microdefects varies for different coating techniques. Although techniques such as ASTM 562-89 exist to quantify porosity within these coatings, microcracks cannot be quantified without transmission electron microscopy (TEM) analysis. Moreover, it is not only the extent but also the shape and size of individual defects that control crack propagation. The presence of secondary phase particles within the microstructure makes the situation complex. A typical composition of WC-Co coating analyzed by XRD indicated crystalline phases such as WC, W, $Co_3W_9C_4$, and W_2C. The extent of these phases was dependent upon the starting powder, coating process, and its parameters. In addition, amorphous phases such as W-Co-C have also been reported in these coatings.[41,42] Such is the complexity of microstructure that stress concentrations are inevitable during cyclic loading. During rolling contact, these microdefects had a higher tendency for crack propagation at the depths of maximum shear stress (τ_{max}) and orthogonal shear stress reversal (τ_{orth}). The depth and magnitude of these shear stresses can be evaluated using the conventional contact mechanics approach,[29] reproduced here for clarity:

$$\tau_{orth} = 0.23 \times P_o \text{ at a depth of } 0.4 \times b \quad \text{(Eq 8)}$$

$$\tau_{max} = 0.35 \times P_o \text{ at a depth of } 0.65 \times b \quad \text{(Eq 9)}$$

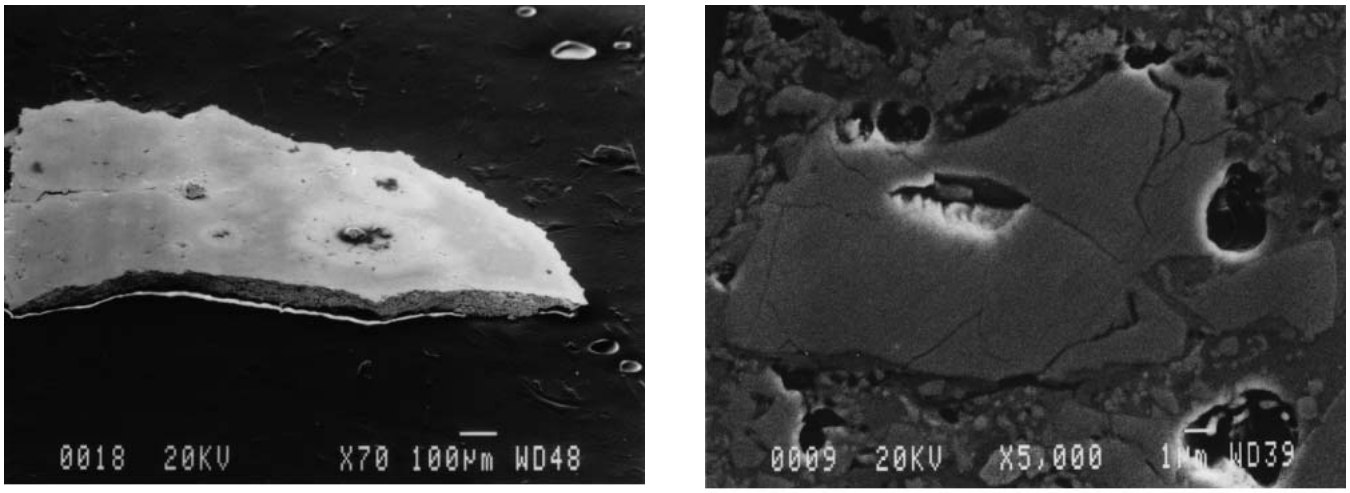

(a) (b)

Fig. 10 Delamination debris and coating microstructure: **(a)** delamination debris (test T6); **(b)** BEI of WC-Co coating produced by D-Gun technique

Similar relations exist for circular contacts. The location of these stresses in the vicinity of coating substrate interface can significantly influence crack propagation because of the mismatch of coating and substrate properties and high level of quenching stress.[43] Surface and subsurface examination of delaminated coatings indicated that circumferential cracks appeared beneath the surface at the depths of maximum shear (90-100 µm) and orthogonal shear (40-50 µm), under the given test conditions of contact stress and configuration, and calculated from Eq 12 and 13. Figure 8(a,b) shows the occurrence of these cracks under the wear track at two different approximate depths of 40 and 90 µm, which can be related to the depth of orthogonal and maximum shear stress, respectively. This behavior was typical of all delamination failures of WC-Co coatings produced by the various spraying processes, whereas for Al_2O_3 coatings, cracks were only observed at the coating-substrate interface near the approximate depth of maximum shear stress. Hence, cohesive and adhesive delamination were observed in cermets, whereas only adhesive delamination existed for ceramic coating.

These cracks extended at their respective depths of either the shear stresses or the coating substrate interface and joined each other if crack propagation brought them in the vicinity of each other (Fig. 8b). The crack propagation, however, continued under the surface (Fig. 8c). The cracks, which were at the approximate depth of orthogonal shear, generally reached the surface leading to the depth of failure of 40-50 µm in most of the cases of coating delamination within the coating microstructure (Fig. 3a and 7a). When the coating thickness was such that the coating substrate interface was at the location of shear stress, crack propagation was accelerated because the mismatch of coating substrate properties and cracks extended to greater lengths. Typical observations of these interfacial cracks are shown in Fig. 8(g,h). Figure 11 shows a schematic of the coating delamination process and the influence of coating thickness on crack propagation, which is based upon the observation of subsurface cracks from various tests during the investigation. This failure mode was, however, absent for the tests conducted below a contact stress of 2 GPa. This was attributed to subcritical stress in-

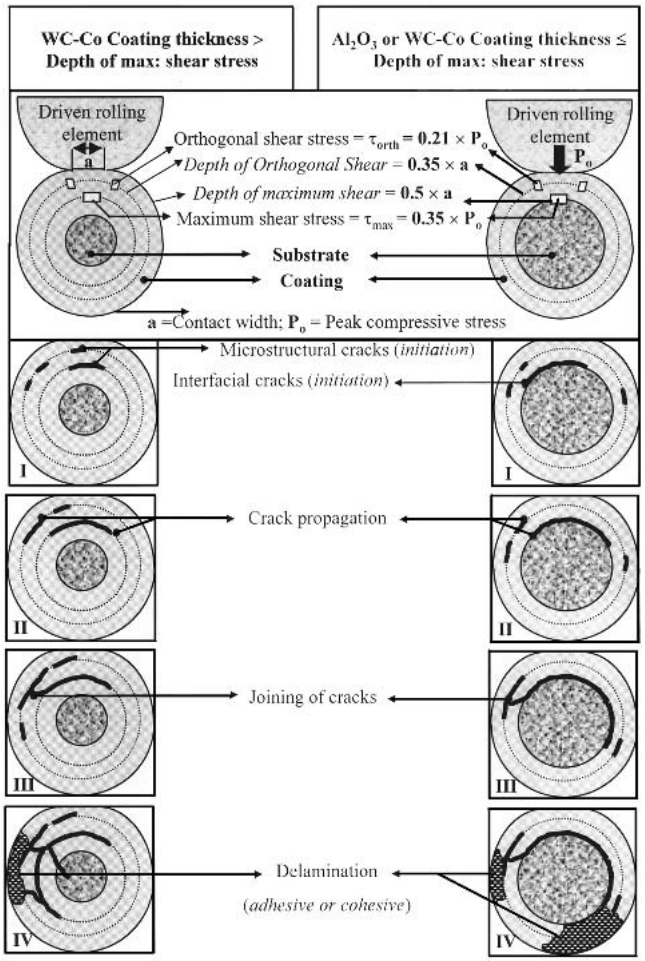

Fig. 11 Schematic of the coating delamination process: **(I)** initiation of cracks at the depths of maximum shear and orthogonal shear stress; **(II)** propagation of cracks parallel to surface; **(III)** combination of cracks; **(IV)** coating delamination

tensity, which was unable to trigger crack propagation either within or at the coating substrate interface, under low stress (<2 GPa) conditions. In addition, the probability of adhesive delamination was low for the tests conducted within the contact stress range of 2-3 GPa, but with a coating thickness greater than the depth of shear stress. This was mainly because of the shift of coating substrate interface away from the location of maximum shear stress.

Another way of avoiding the shear stresses at the coating-substrate interface and combating delamination was to shift the maximum and orthogonal shear stress into the substrate material by choosing much thinner coatings, e.g., around 20 μm under the given tribological conditions (Table 1). This was essentially the intention of the test reported as T5. RCF investigations indicated that coating delamination was indeed absent in those cases of thinner coatings,[18] conducted at low (>2 GPa) stress levels. However, note that such a solution to combat delamination could only be applied to cermet but not ceramic coatings, due to the premature adhesive failure of the latter. In addition, the idea of applying a hard coating in tribological applications is to improve life and minimize the dependency of failure on the substrate material, so that cheaper substrate can be used. This, however, was no longer the case with such thinner coatings, because the shift of shear stresses into the substrate makes their fatigue properties much more important than the coating material, and in a sense, defeats the object of the exercise. Moreover, for the thinner coatings, the interface still poses a crack initiation site, especially because of the higher probability of defects at this location owing to the variations in processing conditions. Hence, such a solution to resist coating delamination can only be safely applied at relatively low stress levels of around 1.5 GPa.

4.2.2 Influence of Coating Material. Although conventional contact mechanics approaches based upon homogenous materials cannot be directly applied to find solutions of layered surfaces, and several authors (Cole et al.,[44] Djabella et al.,[45] Sun et al.,[46] Kapoor et al.,[47] and Lawn et al.[48]) have addressed this problem, an exact solution for thermal spray coatings does not exist to date. Conventional approaches to mimic the stress distribution in thermal spray coatings can, however, be used as a guideline, because the evidence of the depths of crack propagation and Hertzian theory is compelling, as discussed in Section 4.2.1. This was specifically true for coatings thicker than 150 μm under the given test conditions, because the coating substrate interface was far from the Hertzian contact stress distribution pattern. Similarly, the Young's modulus of WC-Co coatings produced by the HVOF technique is generally in the range of 240-260 GPa, as indicated by Brandt[31] and Kuroda et al.[49] Slightly lower values are reported (220 GPa) for WC-Co coatings produced by other techniques. These values of Young's modulus are similar to those in conventional bearing steels (210 GPa); hence the stress field will be marginally affected by the mismatch of elastic properties of coating and substrate materials for the cases, especially when the coating thickness is greater then the depth of maximum shear stress. However, the role of quenching stresses and a contamination layer, along with this mild mismatch of elastic properties at the interface, can significantly affect the stress field, especially for coatings thinner than the depth of maximum shear, and conventional contact mechanics approaches need to be modified. The case is worse for Al_2O_3 coatings because the Young's modulus is generally low, i.e., 110 GPa,[50] which indicates a significant mismatch of elastic properties, especially for the cases when the coating thickness is less than the depth of maximum shear stress. In addition, because of the higher melting point of Al_2O_3 ceramic than that of WC-Co cermet, the quenching stresses will be higher, especially at the coating substrate interface. Hence, for ceramic coating, the coating-substrate interface was the weakest section and showed premature failure regardless of the changes in tribological conditions.

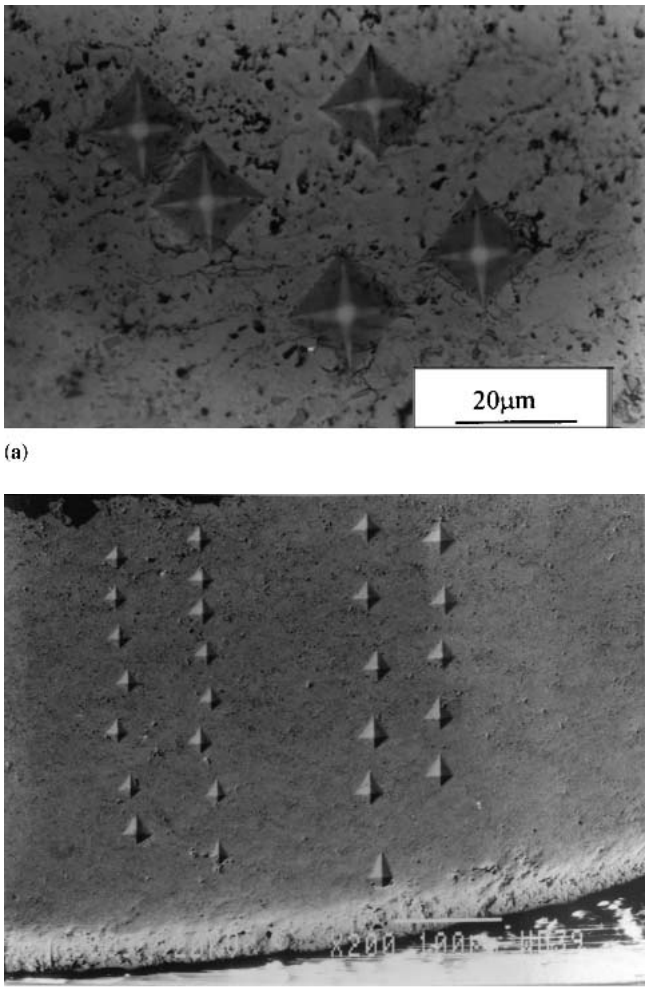

Fig. 12 Fracture toughness behavior of typical HVPS and HVOF coating microstructure in microhardness indentations: **(a)** HVPS coating at indentation load of 2.94 N; **(b)** HVOF coating at indentation loads of 2.94 and 4.9 N

4.2.3 Influence of Coating Process. The investigation of fracture toughness of these coatings illustrates the dependence of coating delamination on fracture toughness. As indicated in Section 4.1, HVOF coatings had the highest resistance of microcracking during an indentation test (Fig. 12). It is for this reason that HVOF coatings thicker than 150 μm resisted adhesive and cohesive delamination up to a stress of around 3 GPa. These coatings did not fracture at indentation loads as high as 500 gm (4.9 N) (Fig. 12a), in comparison to similar coatings produced by HVPS technique (Fig. 12b). Quantitative values of fracture

toughness cannot be obtained because of cracking of coating material from the side of an indentation diagonal rather than from the notch (Fig. 12b). In addition, the indentation cracks did not satisfy the criterion $C > 2d$, where C is the crack length and d is the diagonal of indentation, which must be satisfied for indentation fracture toughness evaluation.[51,52] Hence, high fracture toughness, coupled with the influence of coating thickness, can be used as an index of performance to combat coating delamination.

4.2.4 Interfacial Delamination and Quenching Stress. Another important consideration in combating interfacial delamination is the control of quenching stresses at the coating-substrate interface. Quenching stresses are tensile in nature and are caused by the inelastic behavior of the impacting lamella, because its contraction is constrained by the cold substrate or underlying lamella. Gill[43] described a variety of phenomena that explain the relaxation of these stresses by interfacial sliding and microcracking. Low preheat temperature can thus lead to high quenching stresses because of an increased rate of cooling and poor wettability. Figure 5 shows a typical example in which low preheat temperature led to high quenching stresses and macrocracks at the coating-substrate interface. Cracks originated from the coating-substrate interface and radiated across the wear track to delaminate the coating at the interface. A comparison of Fig. 5 and 6(d) shows the difference in mechanism caused by quenching stresses in the sense that coating delamination occurred not only from the wear track, but also propagated to far greater lengths across the wear track (Fig. 5). Higher preheat temperature thus constrained the delamination (by controlling residual/quenching stress) to within the wear track, with no crack propagation across the wear track. However, too high a preheat temperature can soften the substrate, which can result in failures similar to bulk material failure, as discussed below. Note that if the coating thickness is greater than the depth of the shear stress, and failure is interfacial delamination in the presence of large cracks across the rolling direction (Fig. 5b), then this failure may be considered as an independent failure mode caused by the adhesive failure at the interface caused by high quenching (or residual) stress.

In summary, despite changes in the coating process and material considered in this study, the mechanism of coating delamination was subsurface stress concentrations leading to crack initiation and propagation parallel to the surface. The specifics of the mechanism, however, varied on the basis of coating material, which for the cermets was strongly influenced by the coating thickness and location of maximum and orthogonal shear stress under the contact region. Ceramic coatings, albeit changes in tribological conditions, delaminated at the coating substrate interface.

4.3 Coating Failure Caused by Bulk Deformation

Bulk deformation of substrate material is of primary importance for hard coatings (WC-Co, Al_2O_3) on soft substrates such as mild steel. This is because the contact stress can be in the elastic range of the coating material and in the plastic range of the substrate. The primary effect of this is the plastic flow of substrate, leading to conformity of the contact region, and a hump at the edge of wear track. Figure 4(a,b) shows a typical example of such a failure, in which the substrate could no longer support the coating, leading to bending and cracking of coating material in the initial stages. As cyclic loading continues, the coating cracks in the middle of wear track, as shown in Fig. 4(c), because the coating is unable to plastically deform under tensile stress caused by the plastic flow of substrate material. This plastic flow continues and the substrate is pushed up at the edges of the wear track, leading to subsequent cracking at the edge of wear track, as shown in Fig. 4(a). Further loading leads to the opening of the crack from tension, and the substrate finally emerges at the edge of the wear track as shown at an inclined angle in Fig. 4(b). The crack propagation is progressive because of cyclic loading, thus this failure mode can be categorized as a fatigue failure mode. Once the conformity of contact is such that the stresses in the substrate are no longer in the plastic region, the substrate migration terminates and a steady state is reached.

Figure 13 shows a schematic of this failure mode and indicates that substrate hardness should be carefully selected (on the basis of contact loading) to combat this failure. A similar effect is possible if preheat temperature prior to spraying is too high, because plastic flow of the substrate can increase the tensile stress within the coating material. This effect is more carefully controlled in PVD coatings. The mechanism of bulk deformation is thus strongly dependent upon the ability of substrate material to support the coating in relation to the contact stress, and is marginally affected by the changes either in the coating material or the process.

4.4 Coating Failure Caused by Spalling

Spalling is the most commonly seen failure in conventional steel rolling element bearings. Spalling fatigue, however, is the most rare mode of fatigue failure in thermal spray coatings. Tallian[25] defined a spall as a sharp-edged, steep-walled, flat-bottomed feature formed by the fracture of a surface. Spall in thermal spray coatings resembles in appearance to the spalls in conventional bearings, as shown in Fig. 6(a), and it differs from delamination failure discussed in Section 4.2. The spall is contained within the wear track, and it is circular or elliptical in appearance, with its surface area (width to depth ratio) much smaller than that of a delaminated coating. A comparison of Fig. 5(a) and 6(a) can distinguish the appearance between the two failures. Spalls can initiate from micropits, furrows, grinding marks, or dents on the surface of a wear track. In addition, subsurface inclusions and defects are known to lead to spalling of rolling elements.

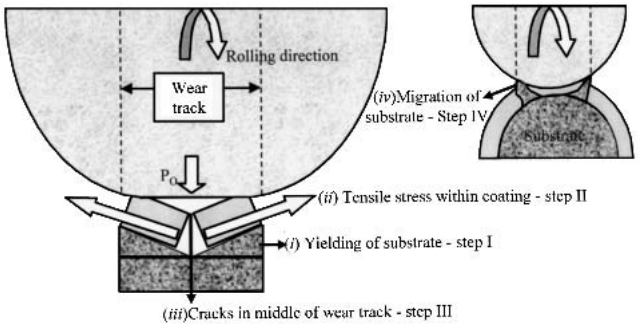

Fig. 13 Mechanism of bulk deformation

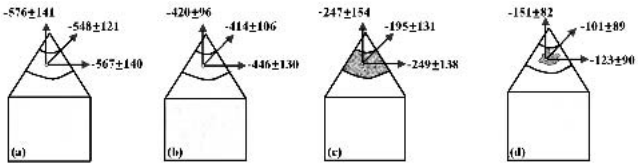

Fig. 14 Residual stress measurement results of HVOF coatings: **(a,b)** before RCF test; **(c)** pitted wear track; **(d)** delaminated area

Examination of the wear track of a spalled specimen (Fig. 6a) indicates that substantial micropitting of the wear track occurred before fatigue spall was produced. This highlights the possibility that the fatigue spall was surface initiated (i.e., from the micropits) and subsequent crack propagation took place as a result of cyclic loading. It is also possible that if the spall was assumed to be surface initiated, HPP could have significantly assisted in crack propagation. The possibility of subsurface cracking leading to fatigue spall can also not be overlooked. However, the exact mechanisms of fatigue spall (i.e., surface or subsurface initiation) and propagation in thermal spray coatings are not completely understood.

Note that spalling of thermal spray coatings was strictly limited to cermet HVOF coatings with no evidence of this failure in ceramics. It could be because HVOF coatings indicated relatively superior fracture toughness compared to other processes, and thus had a greater tendency to fail in spall mode. However, such failures were seldom seen in thermal spray coatings and were also associated with the cases of improved RCF performance.

4.5 Influence of Residual Stress

Figure 14 shows typical results of residual stress measurements on WC-Co coatings produced by the HVOF technique. These coatings showed a compressive residual stress caused by the mismatch of the coefficient in thermal expansion of coating and substrate material (Fig. 14a,b). These compressive residual stresses are protective in nature because they combat tensile cracking. Compressive residual stress fields in conventional steel ball bearings have also significantly improved the bearing life.[53] Similarly, studies by Bush et al.,[54] Zaretsky et al.,[55] Pomeroy et al.,[56] Muro et al.,[57] and Chen et al.[58] indicated that the generation of residual stress in rolling contact could be critical to the RCF performance.

Figure 14(c) shows the residual stress field after the RCF test. The specimen failed because of micropitting of the wear track after 2.7×10^6 stress cycles. Note that the compressive residual stress attenuated during the RCF test. Because the depth of residual stress measurement was near the surface, this attenuation of residual stress further confirmed the microcracking of the coating, leading to micropitting as described in Section 4.1. A similar trend was observed for delaminated areas of coating. Figure 14(d) shows a typical example of residual stress measurement within the delaminated area. The macrocracking observed during the coating delamination attenuated the compressive residual within the coating, because negligible values were obtained within the failed areas. A similar trend was observed for coatings produced by HVPS and D-gun techniques. Al_2O_3 coatings, however, showed a high scatter in the diffraction results. It is believed that amorphous phases were present within the ceramic coating microstructure, which made the diffraction pattern complex, and residual stress evaluations less reliable.

5. Conclusions

- Four modes of fatigue failure were identified as abrasive, delamination, bulk deformation, and spalling. These failure modes compete during fatigue failure and eventual coating failure may be either due to one or a combination of these modes.
- Abrasion is a near-surface type, noncatastrophic failure mode and can be controlled by appropriate selection of contacting pair and lubrication conditions.
- Delamination is a catastrophic failure mode and can be combated by appropriate selection of coating thickness and fracture toughness. This failure mode was absent in the tests conducted below 2.0 GPa of contact stress.
- Bulk failure can be avoided by controlling the hardness of substrate and also increasing the coating thickness.
- Spalling may originate from surface or subsurface and is the least frequently seen failure mode in thermal spray coatings.
- Coating failures were attributed to micro- and macrocracking of either the coating material or the coating substrate interface, which also resulted in the attenuation of compressive residual stress.

Acknowledgment

The authors are most grateful to Prof. Shogo Tobe of Asikaga Institute of Technology, Japan, for his assistance in residual stress measurements.

References

1. H. Aramaki, Y. Shoda, Y. Morishita, and T. Sawamoto: "The Performance of Ball Bearings With Silicon-Nitride Ceramic Balls in High Speed Spindles for Machine Tools," *J. Tribology*, 1988, *110*, pp. 693-98.
2. W.D. Sproul and P.J. Rudnik: "Ceramic Coated Bearing Elements for Improved Durability and Reliability," Final Report for Contract F33615-92-C-5295, Advanced Projects Research Agency (APRA), USA, 1994.
3. A. Nakajima, T. Mawatari, M. Yoshida, K. Tani, and A. Nakahira: "Effects of Coating Thickness and Slip Ratio on Durability of Thermally Sprayed WC Cermet Coatings in Rolling/Sliding Contact," *Wear*, 2000, *241*, pp. 166-73.
4. B.Y. Sarma and M.M. Mayuram: "Some Studies on Life Prediction of thermal Sprayed Coatings Under Rolling Contact Conditions," *J. Tribology*, 2000, *122*(3), pp. 503-10.
5. R. Ahmed and M. Hadfield: "Failure Modes of Plasma Sprayed WC-Co Coated Rolling Elements," *Wear*, 1999, *230*, pp. 39-55.
6. M.Y. He, A.G. Evans, and J.W. Hutchinson: "Interface Cracking Phenomena in Constrained Metal Layers," *Acta Mater*., 1996, *44*(7), pp. 2963-71.
7. X.H. Liu, Z. Suo, Q. Ma, and H. Fujimoto: "Cracking and Debonding in Integrated Microstructures," *Material Research Society Symposium Proceedings*, 1998, Materials Research Society, USA, *516*, pp. 313-24.
8. D.A.J. Ramm, I.M. Hutchings, and T.W. Clyne,: "Erosion Resistance

and Adhesion of Composite Metal/Ceramic Coatings Produced by Plasma Spraying, " *J. Phys. IV*, 1993, *3*(7), pp. 913-19.
9. M. Yoshida, K. Tani, A. Nakahira, A. Nakajima, and T. Mawatari: "Durability and Tribological Properties of Thermally Sprayed WC Cermet Coating in Rolling/Sliding Contact" in *Thermal Spraying: Current Status and Future Trends*, A. Ohmri, ed., High Temperature Society of Japan, Osaka University, Osaka, Japan, 1995, pp. 663-68.
10. R. Nieminen, K. Vuoristo, K. Niemi, and T. Mantyla: "Rolling Contact Fatigue Characteristics of Thermal Spray Coatings" in *Thermal Spray Science and Technology*, C.C. Berndt and S. Sampath, ed., ASM International, Materials Park, OH, 1995, pp. 651-57.
11. V.H.S. Wilms: "The Microstructure of Plasma Sprayed Coatings," Ph.D. Thesis, SUNY at Stony Brook, Stony Brook, NY, 1978.
12. V.V. Kudinov, P.Y. Pekshev, and V.A. Safiullin: "Forming of the Structure of Plasma-Sprayed Materials, High Temperature Dust Laden Jets," Solonenko and Fedorchenko, ed., VSP Holland, 1989, pp. 381-418.
13. P. Vuoristo, K. Niemi, A. Makela, and T. Mantyla: "Spray Parameter Effects on Structure and Wear Properties of Detonation Gun Sprayed WC+17%Co Coatings" in *Thermal Spray: Research Design and Applications*, C.C. Berndt and T.F. Bernecki, ed., ASM International, Materials Park, OH, 1993, pp. 173-78.
14. R. Tourret and E.P. Wright: "Rolling Contact Fatigue: Performance Testing of Lubricants," *International Symposium, I. Petroleum*, Heyden & Son Ltd., London, 1977.
15. Scott, D., & Blackwell, J. "Hot Pressed Silicon Nitride as a Rolling Bearing Material—a Preliminary Assessment," *Wear*, 1973, *24*, pp. 61-67.
16. R. Ahmed and M. Hadfield: "Rolling Contact Fatigue Behaviour of Thermally Sprayed Rolling Elements," *Surf. Coat. Technol.*, 1996, *82*, pp. 176-86.
17. B.O. Jacobson: *Rheology and Elasto-Hydrodynamic Lubrication*, Baker & Taylor, Charlotte, NC, 1991.
18. R. Ahmed and M. Hadfield: "Wear of HVOF Coated Cones in Rolling Contact," *Wear*, 1997, *203-204*, pp. 98-106.
19. R. Ahmed and M. Hadfield: "Fatigue Behaviour of HVOF Coated M-50 Steel Rolling Elements," *Surf. Eng.*, 1998, *14*(6), pp. 473-80.
20. R. Ahmed and M. Hadfield: "Experimental Measurement of Residual Stress Field Within Thermally Sprayed Rolling Elements," *Wear*, 1997, *209*, pp. 84-95.
21. G.H. Farrahi, P.H. Markho, and G. Maeder: "A Study of Fretting Wear With Particular Reference to Measurement of Residual Stress by X-ray Diffraction," *Wear*, 1991, *148*, pp. 249-60.
22. B.D. Cullity: *Elements of X-ray Diffraction*, Addison-Wesley, Reading, MA, 1978.
23. K.L. Johnson: *Contact Mechanics*, Cambridge University Press, New York, 1985.
24. W.E. Littmann and R.L. Winder: "Propagation of Contact Fatigue From Surface and Subsurface Origins," *Trans. ASME*, 1966, *September*, pp. 624-36.
25. T.E. Tallian: "On Competing Failure Modes in Rolling Contact," *Trans. ASLE*, 1967, *10*, pp. 418-39.
26. W.E. Littmann: "The Mechanism of Contact Fatigue," *Conference on Approach to Lubrication of Concentrated Contacts*, NASA, 1970, pp. 309-77.
27. K.L. Johnson, J.A. Greenwood, and S.Y. Poon: "A Simple Theory of Asperity Contact in Elastohydrodynamic Lubrication," *Wear*, 1972, *19*, pp. 91-108.
28. D. Berthe, L. Flamand, and M. Godet: "Micropitting in Hertzian Contacts," *J. Lubr. Technol.*, 1980, *102*, pp. 479-85.
29. Engineering Science Data Units, ESDU-84017, "Contact Phenomena—II: Stress Fields and Failure Criterion in Concentrated Elastic Contacts Under Combined Normal and Tangential Loading," ESDU International, USA, 1984.
30. R.C. Tucker Jr.: "Structure Property Relationship in Deposits Produced by Plasma Spray & Detonation Gun Techniques," *J. Vac. Sci. Technol.*, 1994, *11*, pp. 725-34.
31. O.C. Brandt: "Mechanical Properties of HVOF Coatings," *J. Thermal Spray Technol.*, 1995, *4*, pp. 147-52.
32. R.S. Sayles: "Debris and Roughness in Machine Element Contacts: Some Current and Future Engineering Implications," *J. Eng. Tribol.*, 1995, *209*(3), pp. 149-72.
33. A.V. Oliver, A.H. Spikes, and P.B. Macpherson: "Wear in Rolling Contacts," *Wear*, 1986, *112*, pp. 121-44.
34. E. Way: "Pitting Due to Rolling Contact," *J. Appl. Mech.*, 1935, *2*, pp. A49-A58.
35. R. Ahmed and M. Hadfield: "Rolling Contact Fatigue Performance of Plasma Sprayed Coatings," *Wear*, 1998, *220*, pp. 80-91.
36. N.P. Suh: "An Overview of the Delamination Theory of Wear," *Wear*, 1977, *44*, pp. 1-16.
37. J.W. Flemming and N.P. Suh: "Mechanics of Crack Propagation in Delamination Wear," *Wear*, 1977, *44*, pp. 39-56.
38. N.P. Suh and N. Saka: "Fundamentals of Tribology," *International Conference on the Fundamentals of Tribology*, MIT Press, Boston, 1980.
39. N.P. Suh: *Tribophysics*, Prentice Hall, New York, 1986.
40. P.J. Rabier: "Some Remarks on Damage Theory," *Int. J. Eng. Sci.*, 1989, *27*, pp. 29-54.
41. H.L. Villers Lovelock: "Powder/Processing/Structure Relationships in WC-Co Thermal Spray Coatings: A Review of the Published Literature," *J. Thermal Spray Technol*., 1998, *7*(3), pp. 357-73.
42. M.D.F. Harvey, A.J. Sturgeon, F.J. Blunt, and S.B. Dunkerton: Investigation Into the Relationship Between Fuel Gas Selection, Wear Performance, and Microstructure of HVOF Sprayed WC-Co Coatings, in *Thermal Spraying: Current Status and Future Trends*, A. Ohmri, ed., High Temperature Society of Japan, Osaka University, Osaka, Japan, 1995, pp. 471-6.
43. S.C. Gill: "Residual Stress in Plasma Sprayed Deposits," Ph.D. Thesis, Gonville and Caius College Cambridge, U.K., 1993.
44. S.J. Cole and R.S. Sayles: "A Numerical Model for the Contact of Layered Elastic Bodies With Real Rough Surfaces," *Trans. ASME*, 1992, *114*, pp. 334-40.
45. H. Djabella and R.D. Arnell: "Finite Element Analysis of Elastic Stresses in Multilayered Systems," *Thin Solid Films*, 1994, *245*, pp. 27-33.
46. Y. Sun, A. Bloyce, and T. Bell: "Finite Element Analysis of Plastic Deformation of Various TiN Coating/Substrate Systems Under Normal Contact With a Rigid Sphere," *Thin Solid Films*, 1995, *271*, pp. 122-31.
47. A. Kapoor and J.A. Williams: "Shakedown Limits in Rolling-Sliding Point Contacts on an Anisotropic Half Space," *Tribol. Int.,* 1996, *191*(1-2), pp. 256-60.
48. B.R. Lawn, N.P. Padture, F. Guiberteau, and H. Cai: "Model for Microcrack Initiation and Propagation Beneath Hertzian Contacts in Polycrystalline Ceramics," *Acta Mater*., 1994, *42*(5), pp. 1683-93.
49. S. Kuroda and T.W. Clyne: "Quenching Stress in Thermally Sprayed Coatings," *Thin Solid Films*, 1991, *200*, pp. 49-66.
50. R. Kawase and K. Tanaka: "Study on Elastic Constant and Residual Stress Measurements During Ceramic Coatings" in *Thermal Spray Research and Applications*, T.F. Bernecki, ed., ASM International, Materials Park, OH, 1990, pp. 339-42.
51. C.K. Lin and C.C. Berndt: "Measurement and Analysis of Adhesion Strength for Thermally Sprayed Coatings," *J. Thermal Spray Technol.*, 1994, *3*(1), pp. 75-104.
52. C.K. Lin, S.H. Leigh, and C.C. Brendt: Investigation of Plasma Sprayed Materials by Vickers Indentation Tests, in *Thermal Spraying: Current Status and Future Trends*, A. Ohmri, ed., High Temperature Society of Japan, Osaka University, Osaka, Japan, 1995, pp. 903-08.
53. J.C. Clark: "Fracture Tough Bearings for High Stress Applications," *Proceedings of the 21st Joint Propulsion Conference*, Paper AIAA-85-1138, 1985.
54. J.J. Bush, W.L. Grube, and G.H. Robinson: "Microstructural and Residual Stress Changes in Hardened Steel Due to Rolling Contact" in *Rolling Contact Phenomena*, 1962, pp. 365-99.
55. E.V. Zaretsky, R.J. Parker, and W.J. Anderson: "A Study of Residual Stress Induced During Rolling Contact," *J. Lubr. Technol.*, 1969, *91F*, pp. 314-19.
56. R.J. Pomeroy and K.L. Johnson: "Residual Stresses in Rolling Contact," *J. Strain Anal.*, 1969, *4*(3), pp. 208-18.
57. H. Muro, N. Tsushima, and K. Nunome: "Failure Analysis of Rolling Bearings by X-ray Measurement of Residual Stress," *Wear*, 1973, *25*, pp. 345-56.
58. Q. Chen, G.T. Hahn, C.A. Rubin, and V. Bhargava: "The Influence of Residual Stresses in Rolling Contact Mode II Driving Force in Bearing Raceways," *Wear*, 1988, *126*, pp. 17-30.